Published in IET Power Electronics
Received on 23rd April 2011
Revised on 27th July 2011
doi: 10.1049/iet-pel.2011.0194

ISSN 1755-4535

High-efficiency bidirectional dc–dc converter with high-voltage gain

R.-J. Wai[1] *R.-Y. Duan*[2] *K.-H. Jheng*[1]

[1]*Department of Electrical Engineering, Yuan Ze University*
[2]*Department of Safety, Health and Environmental Engineering, Hung Kuang University*
E-mail: rjwai@saturn.yzu.edu.tw

Abstract: The aim of this study is to develop a high-efficiency bidirectional dc–dc converter for a power storage system. The proposed converter can boost the voltage of an energy-storage module (e.g. battery) to a high-voltage-side dc bus for the load demand. When the high-voltage-side dc bus has excess energy, this energy-storage module can be charged by the dc bus. In this study, a coupled-inductor bidirectional converter scheme utilises only three power switches with the properties of voltage clamping, synchronous rectification and soft switching. As a result, the objectives of high-voltage gain, high-efficiency power conversion and bidirectional power control can be achieved. Some experimental results via a 48/360 V kW-level prototype are given to verify the effectiveness of the proposed converter in practical applications.

1 Introduction

In recent years, the development of bidirectional dc–dc converters has become urgent for clean-energy vehicle applications, because battery-based energy storage systems are required to cold start and battery recharge. However, back-up power from the battery is supplied by using a bidirectional converter, which is employed in many uninterrupted power supplies (UPS), aerospace power systems and industrial applications. The dc back-up energy system normally consists of numerous typical low-voltage-type batteries. Although series strings of storage batteries can provide a high voltage, slight mismatches or temperature differences cause charge imbalance if the series string is charged as a unit [1]. Charge equalisation cycles must be used in an attempt to correct imbalance, but conventional approaches to this process stress the batteries, shorten their life and are not always effective. Nowadays, the extensive operation of batteries in parallel strings stems from the desire of enhancing the redundancy of the power supply from the battery, and the problems induced by series strings of storage batteries could be alleviated [2]. However, the output voltage remains low by this parallel connection way. Therefore a high-efficiency bidirectional dc–dc converter with high-voltage diversity is a key component of batteries connected in parallel.

Bidirectional dc–dc converters with transformer-based structures are probably the most popular topologies [3–13], and soft-switching techniques are usually applied to reduce the corresponding switching losses. These mechanisms with isolated transformers have high conduction losses because the usual number of power switches is between four and nine. Accordingly, practical implementation is complicated and expensive. Nowadays, switched-capacitor dc–dc converters [14, 15] have attracted much attention as an alternative means of providing bidirectional power flow control. However, increased switching loss and current stress are the critical drawbacks, and the major challenge is to design a circuit with few switch devices and capacitors. Generally speaking, the bidirectional converter in the UPS must have a high step-up/step-down voltage gain. Zhao and Lee [16] introduced a family of high-efficiency, high step-up dc–dc converters by adding only one additional diode and a small capacitor. It can recycle the leakage energy and mitigate the reverse-recovery problem. Inaba *et al.* [17] introduced a two-quadrant PWM chopper-type dc–dc converter via a coupled inductor. In this technique, only three switches were applied to achieve bidirectional power flow. Although an additional snubber capacitor was successfully used to clamp the spike voltage, a 250 V voltage-rated switch was employed in a low-voltage (36 V) side circuit, resulting in a large conduction loss because a switch with a higher $R_{DS(ON)}$ was used. Coupled inductors with a lower-voltage-rated (80 V) switch and a passive regenerative snubber circuit [18, 19] were adopted to realise that the high-voltage gain with a 400 V output voltage, and the performance was superior to that in [17]. Unfortunately, these non-isolation topologies presented in [16, 18, 19] only control unidirectional power flow. Yu *et al.* [20] introduced an ultra-high-efficiency bidirectional dc–dc converter constructed by the coupled inductor with the interleaved topology. Although this topology with soft switching can achieve the goal of high-efficiency power conversion, many series strings of storage batteries are required to reduce the input/output voltage diversity. Wu *et al.* [21] investigated a bidirectional dc–dc converter with a flyback snubber. Although this topology has the properties of soft start-up, active snubber and high step-up voltage gain, this

© The Institution of Engineering and Technology 2011

combination scheme with two converters is complicated so that the goal of high-efficiency power conversion is difficult to achieve and its cost is inevitably increased. Chen *et al.* [22] presented a snubberless bidirectional dc–dc converter with a new CLLC resonant tank. Although this additional CLLC resonant tank was successfully designed to minimise the corresponding switching losses, the values of capacitor and inductor should be strictly considered for all switches operated with the property of soft switching.

This study presents a bidirectional converter with a coupled inductor, which uses only three switches to achieve the high step-up and step-down properties. The techniques exploited in this circuit include the soft switching, synchronous rectification and voltage clamping to reduce the switching and conduction losses by the utilisation of a low-voltage-rated device with a small $R_{DS(on)}$. The windings of the coupled inductor act as a bidirectional magnetic switch to control the release or storage of energy. Since the slew rate of the current change in the coupled inductor is restricted by the leakage inductor, the current transition time to both sides easily enables the switches with soft-switching property. The problems of the saturation and imbalance of the magnetising current for a variable voltage source are prevented. Moreover, a full copper film and the fewer primary-winding turns reduce the size, cost and copper loss of the coupled inductor; the corresponding voltage gain, related to the turns ratio and the duty cycle, is higher than those in previous works [16–18]. Additionally, the stray inductance energy and diode reverse-recovery current problems in conventional converter strategies can also be solved, so that high-efficiency power conversion can be achieved.

2 Converter operations

The system configuration for the proposed bidirectional converter topology is depicted in Fig. 1. The system contains five parts including a low-voltage-side circuit (LVSC), a clamped circuit, a middle-voltage circuit, a step-down circuit and a high-voltage-side circuit (HVSC). The major symbol representations are summarised as follows. V_{bat} (i_{bat}) and V_{bus} (i_{bus}), respectively, denote the voltages (currents) of power sources at the LVSC and HVSC. C_{bat} and C_{bus} are the filter capacitors of the power sources at the LVSC and HVSC, respectively. L_P and L_S represent individual inductors in the primary and secondary sides of the coupled inductor (T_r), respectively, where the primary side is connected to a battery module. An auxiliary inductor in the step-down circuit is denoted as L_2. The symbols, S_1, S_2 and S_3, are the low-voltage switch, the step-down switch and the high-voltage switch, respectively. When the power flows from the HVSC to the LVSC (all switches are active), the circuit works in the buck state to recharge the battery from HVSC or from absorbing regenerated energy. In the other direction of power flow, only trigging the low-voltage switch (S_1) and the high-voltage switch (S_3), the circuit works in boost state to keep the HVSC voltage at a desired value.

The corresponding equivalent circuits as shown in Figs. 2*a* and *b* are used to define the voltage polarities and current directions in the buck and boost states, respectively. The coupled inductor in Fig. 1 can be modelled as an ideal transformer including the magnetising inductors (L_{mp} and L_{ms}) and leakage inductors (L_{kp} and L_{ks}) in Fig. 2. The turns ratio (N) and coupling coefficients (k_p and k_s) of this ideal transformer are defined as

$$N = N_2/N_1 \tag{1}$$

$$k_p = L_{mp}/(L_{kp} + L_{mp}) = L_{mp}/L_P \tag{2}$$

$$k_s = L_{ms}/(L_{ks} + L_{ms}) = L_{ms}/L_S \tag{3}$$

where N_1 and N_2 are the winding turns in the primary and secondary sides of the coupled inductor (T_r). In this study, the following assumptions are made to simplify the converter analyses: (i) All MOSFETs (including their body diodes) are assumed to be ideal switching elements. (ii) The conductive voltage drops of the switch and diode are neglected. The converter design and analyses procedure in the buck and boost states are described in the following subsections.

2.1 Buck state

The characteristic waveforms of the proposed converter in the buck state are depicted in Fig. 3*a* and the topological modes in one switching cycle are expressed as follows.

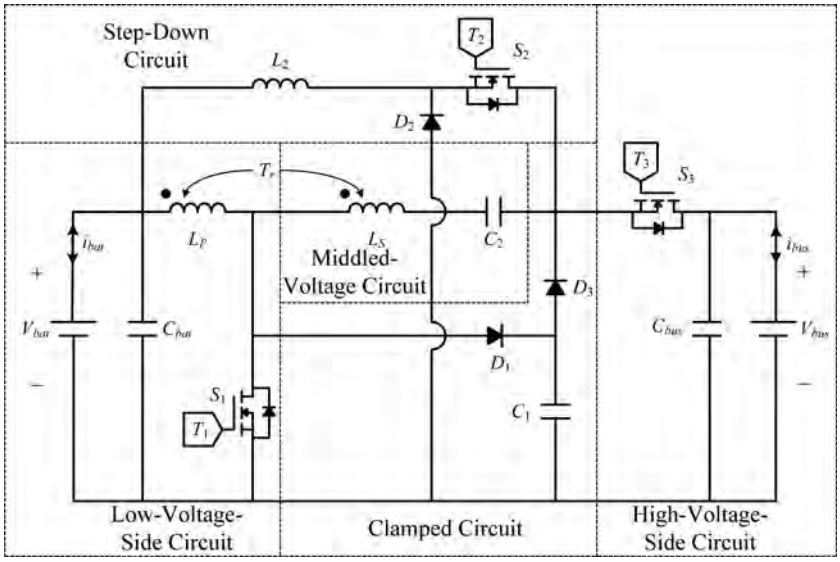

Fig. 1 *System configuration of bidirectional converter*

© The Institution of Engineering and Technology 2011
IET Power Electron., 2012, Vol. 5, Iss. 2, pp. 173–184
doi: 10.1049/iet-pel.2011.0194

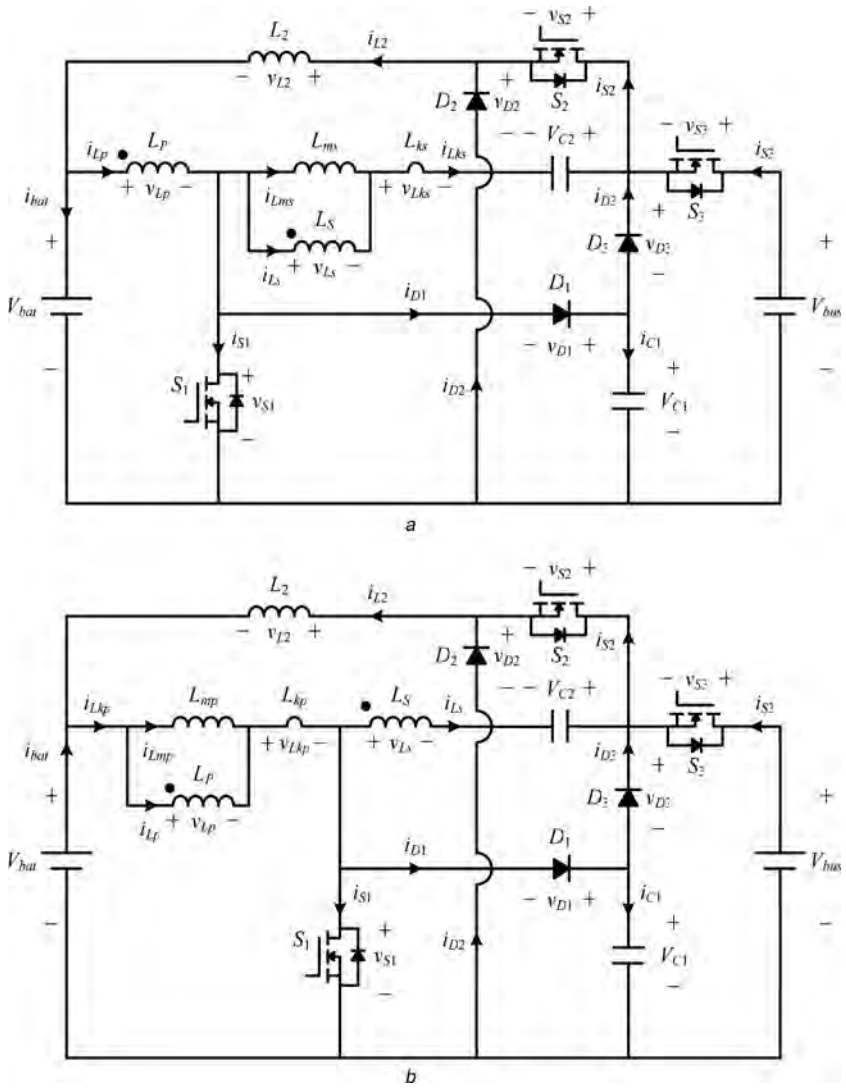

Fig. 2 *Equivalent circuit*

a Buck state
b Boost state

2.1.1 Mode 1 (t_0–t_1): In this mode, the high-voltage switch (S_3) was turned on and the other switches (S_1 and S_2) were turned off for a span. The current (i_{Lks}) is from the HVSC by way of the middle-voltage capacitor (C_2) and two series windings (L_S and L_P) of the coupled inductor (T_r) to charge the battery in the LVSC. According to Kirchhoff's voltage law, the voltage V_{bus} can be given by

$$V_{bus} = V_{C2} - v_{Lks} - v_{Ls} - v_{Lp} + V_{bat} \tag{4}$$

Since $v_{Lks} = v_{Ls}(1 - k_s)/k_s$ and $v_{Lp} = (1/N)v_{Ls}$, (4) can be rearranged as

$$V_{bus} = V_{C2} + V_{bat} - v_{Ls}(k_s + N)/k_s N \tag{5}$$

From (5), one can obtain

$$v_{Ls} = k_s N(V_{bat} + V_{C2} - V_{bus})/(k_s + N) \tag{6}$$

According to Kirchhoff's current law, the current i_{Lks} can be given by

$$i_{Lks} = i_{Lp} = Ni_{Ls} \tag{7}$$

Moreover, the inductor current (i_{L2}) flows through the diode (D_2) to charge the battery so that the voltage across the inductor (L_2) is equal to the negative battery voltage ($-V_{bat}$), and the battery charge current (i_{bat}) is equal to $i_{L2} - i_{Lp}$. In addition, the voltage across the low-voltage switch (S_1) can be obtained as $v_{S1} = V_{bat} - v_{Lp}$.

2.1.2 Mode 2 (t_1–t_2): At time $t = t_1$, the high-voltage switch (S_3) is turned off. Before the diode (D_3) turns on, the parasitic capacitor of the switch (S_2) releases its stored energy to the middle-voltage capacitor (C_2). When the diode (D_3) turns on, the voltage of the switch (S_2) is equal to voltage (V_{C1}). Thus, it results in a lower switch voltage (v_{S2}) before the step-down switch (S_2) is turned on. This situation is similar to the condition of zero-voltage-switching (ZVS), and it is helpful to reduce the switching loss. Since the leakage inductor (L_{ks}) must release the stored energy for a span, the current (i_{Lks}) continues to conduct through the diode (D_3) and the clamped capacitor (C_1). When the current amplitude (i_{Lks}) gradually decreases, the primary current (i_{Lp}) increases via a path through the body diode of the low-voltage switch (S_1). During this interval, the voltage across the switch (v_{S1}) gradually

© The Institution of Engineering and Technology 2011

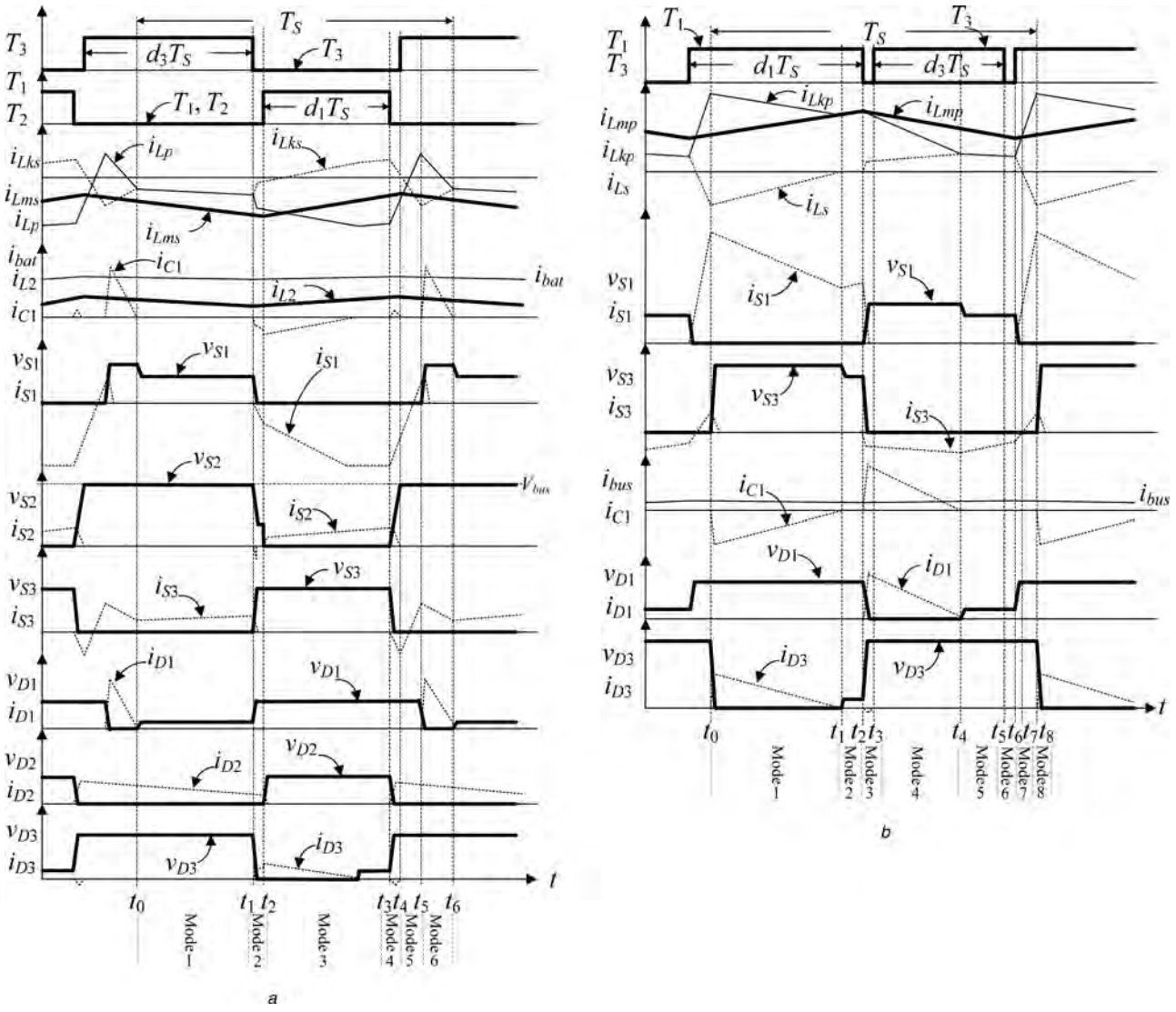

Fig. 3 *Characteristic waveforms of bidirectional converter*
a Buck state
b Boost state

decays to zero. Moreover, the current (i_{L2}) passes through the diode (D_2) in the step-down circuit to charge the battery.

2.1.3 Mode 3 (t_2–t_3): This mode begins when the switches S_1 and S_2 are triggered. Note that, the low-voltage switch (S_1) operates in the synchronous rectified mode with the condition of ZVS, which is useful to reduce the conduction and switching losses for a large current in the LVSC. When the step-down switch (S_2) is turned on with a similar condition of ZVS, the energy stored in the clamped capacitor (C_1) and the middle-voltage capacitor (C_2) is released to the inductor (L_2) and the battery. The current of the switch (S_2) is equal to i_{L2} at this mode. The voltage across the inductor (L_2) can be denoted as $v_{L2} = V_{C1} - V_{\text{bat}}$. According to Kirchhoff's voltage law, the voltage V_{bat} can be represented as

$$V_{\text{bat}} = v_{Lp} + v_{Ls} + v_{Lks} - V_{C2} + V_{C1} \tag{8}$$

Due to $v_{Lks} = v_{Ls}(1 - k_s)/k_s$ and $v_{Lp} = (1/N)v_{Ls}$, the voltage v_{Ls} can be given by

$$v_{Ls} = k_s N(V_{\text{bat}} + V_{C2} - V_{C1})/(k_s + N) \tag{9}$$

Since the voltage across the primary winding (v_{Lp}) is equal to the battery voltage, the voltage V_{bat} can be expressed as

$$V_{\text{bat}} = k_s(V_{C2} - V_{C1})/N \tag{10}$$

2.1.4 Mode 4 (t_3–t_4): At time $t = t_3$, the switches (S_1 and S_2) are turned off. Moreover, the diode (D_2) is conducted to maintain the charge path of the inductor (L_2). Since the leakage inductor (L_{ks}) must release the stored energy for a span, the current (i_{Lks}) continues to conduct through the body diode of the high-voltage switch (S_3). Consequently, the polarities across the primary and secondary windings of the coupled inductor are reversed because of $V_{\text{bus}} > V_{\text{bat}}$. In addition, the body diode of the low-voltage switch (S_1) is conducted to support the summation of the currents i_{Lp} and i_{Lks}.

2.1.5 Mode 5 (t_4–t_5): At time $t = t_4$, the high-voltage switch (S_3) is turned on under the condition of ZVS. It

© The Institution of Engineering and Technology 2011

doi: 10.1049/iet-pel.2011.0194

provides a magnetising path for the coupled inductor (T_r) so that the inductor L_{ms} magnetises again, and the primary current (i_{Lp}) gradually increases. Since the non-dotted point voltage of the primary winding is positive, the body diode of the low-voltage switch (S_1) is turned off, and the primary current (i_{Lp}) charges to the parasitic capacitor of the low-voltage switch (S_1).

2.1.6 Mode 6 (t_5–t_6): At time $t = t_5$, the clamped diode (D_1) is turned on because the voltage of the low-voltage switch (v_{S1}) is higher than the voltage of the clamped capacitor (V_{C1}). Since the capacity of the clamped capacitor (C_1) is large, its voltage (V_{C1}) can be considered as a constant value. By applying Kirchhoff's voltage law, the voltage V_{C1} can be represented as

$$V_{C1} = k_s(V_{bus} - V_{bat} - V_{C2})/(k_s + N) + V_{bat} \quad (11)$$

When the primary current (i_{Lp}) is decreasing and its value equals the current (i_{Lks}), the clamped diode (D_1) is turned off. After that, it begins the next switching cycle and repeats the operation in mode 1.

For easy to analyse, the duty cycles of these switches (S_1 and S_2) are defined as d_1, and the other duty cycle d_3 of the high-voltage switch (S_3) is approximately equal to $1 - d_1$ by neglecting the dead time. Moreover, the coupling coefficient (k_s) is approximated to be one because the voltage gain is less sensitive to the coupling coefficient and the clamped capacitor (C_1) is appropriately selected to completely absorb the leakage inductor energy [18, 19]. By using the voltage-second balance, the relation to the inductor voltage (v_{L2}) can be represented as

$$(V_{C1} - V_{bat})(1 - d_3) = V_{bat}d_3 \quad (12)$$

Similarly, the relation to the second-winding voltage (v_{Ls}) can be expressed by (6) and (9) as

$$(V_{bat} + V_{C2} - V_{bus})d_3 + (V_{bat} + V_{C2} - V_{C1})(1 - d_3) = 0 \quad (13)$$

The voltage gain (G_{V1}) of the proposed converter in the buck state can be obtained by (10), (12) and (13) as

$$G_{V1} = \frac{V_{bat}}{V_{bus}} = \frac{d_3(1 - d_3)}{N(1 - d_3) + 1} \quad (14)$$

2.2 Boost state

When the proposed converter operates in the boost state, the power flow is from the LVSC to the HVSC. Therefore the step-down circuit is not necessary. The characteristic waveforms in the boost state are depicted in Fig. 3*b*, and the topological modes in one switching cycle are described as follows.

2.2.1 Mode 1 (t_0–t_1): In this mode, the low-voltage switch (S_1) was turned on for a span. Since the inductor (L_P) is charged by the battery, the magnetising current (i_{Lmp}) increases gradually in an approximately linear way. The secondary voltage (v_{Ls}) and the clamped capacitor voltage (V_{C1}) are connected in series to charge the middle-voltage capacitor (C_2) through the switch (S_1) and the diode (D_3). Thus, the magnitude of the secondary current (i_{Ls}) is decreased since the voltage of the middle-voltage capacitor (V_{C2}) is increased gradually. According to Kirchhoff's voltage law, the voltage V_{bat} can be given by

$$V_{bat} = v_{Lp} + v_{Lkp} + v_{Ls} - V_{C2} + V_{C1} \quad (15)$$

Since $v_{Lkp} = v_{Lp}(1 - k_p)/k_p$ and $v_{Ls} = Nv_{Lp}$, (15) can be rearranged as

$$V_{bat} = V_{C1} - V_{C2} + v_{Lp} + v_{Lp}(1 - k_p)/k_p + Nv_{Lp} \quad (16)$$

From (16), one can obtain

$$v_{Lp} = k_p(V_{bat} + V_{C2} - V_{C1})/(1 + Nk_p) \quad (17)$$

Owing to $V_{C2} = v_{Ls} + V_{C1}$ and $v_{Ls} = Nv_{Lp}$, the voltage across the middle-voltage capacitor (V_{C2}) can be represented as

$$V_{C2} = v_{Ls} + V_{C1} = Nk_pV_{bat} + V_{C1} \quad (18)$$

Since the current (i_{Lkp}) is the summation of the complementary currents (i_{Lmp} and i_{Lp}), the current curve of i_{Lkp} is similar to a square wave. At the same reason, the switch current (i_{S1}) is also close to a square curve because the switch current (i_{S1}) is equal to the current summation of i_{Lkp} and i_{Ls}. The square current (i_{Lkp}) will result in lower copper and core losses in the coupled inductor. The conduction loss of the switch can be alleviated by the square switch current (i_{S1}).

2.2.2 Mode 2 (t_1–t_2): At time $t = t_1$, the clamped capacitor (C_1) releases its stored energy to zero, the magnitude of the secondary current (i_{Ls}) decays to zero and the diode (D_3) is turned off. At the same time, the low-voltage switch (S_1) is persistently turned on. Thus, the battery provides a magnetising path for the primary winding and the leakage inductor (L_{mp} and L_{kp}) of the coupled inductor in this mode.

2.2.3 Mode 3 (t_2–t_3): At time $t = t_2$, the low-voltage switch (S_1) is turned off. When the voltage across the low-voltage switch (v_{S1}) is higher than the voltage across the clamped capacitor (V_{C1}), the diode (D_1) is conducted to transmit the energy of the primary-side leakage inductor (L_{kp}) into the clamped capacitor (C_1). When the leakage energy has released from the primary side of the coupled inductor, the secondary current (i_{Ls}) is induced in reverse and flows through the body diode of the high-voltage switch (S_3) to the HVSC from the energy of the magnetising inductor (L_{mp}) through the ideal transformer. According to Kirchhoff's voltage law, the voltage V_{bus} can be given by

$$V_{bus} = V_{C2} - v_{Lkp} - v_{Ls} - v_{Lp} + V_{bat} \quad (19)$$

By using (19), $v_{Lkp} = v_{Lp}(1 - k_p)/k_p$ and $v_{Ls} = Nv_{Lp}$, one can obtain

$$v_{Lp} = k_p(V_{bat} + V_{C2} - V_{bus})/(1 + Nk_p) \quad (20)$$

Since the voltage across the low-voltage switch (v_{S1}) is equal to the voltage across the clamped capacitor (V_{C1}), the voltage V_{C1} can be expressed as

$$V_{C1} = V_{bat} - v_{Lp} \quad (21)$$

© The Institution of Engineering and Technology 2011

Substitute (20) into (21), one can obtain

$$V_{C1} = k_p(V_{bus} - V_{bat} - V_{C2})/(1 + Nk_p) + V_{bat} \quad (22)$$

2.2.4 Mode 4 (t_3–t_4): At time $t = t_3$, the high-voltage switch (S_3) is turned on under the synchronous rectified mode with the condition of ZVS because the body diode of the high-voltage switch (S_3) has been conducted by the secondary current (i_{Ls}) in the last mode. In this mode, the current (i_{Lkp}) should be continuously decreased in order to release the energy stored in the leakage inductor (L_{kp}) persistently. Moreover, the secondary current (i_{Ls}) continues to flow through the high-voltage switch (S_3) to the HVSC from the energy of the magnetising inductor (L_{mp}) through the ideal transformer.

2.2.5 Mode 5 (t_4–t_5): At time $t = t_4$, the clamped diode (D_1) is turned off because the current (i_{Lkp}) equals the secondary current (i_{Ls}). Since the clamped diode (D_1) can be selected as a low-voltage Schottky diode, it will be cut off promptly without a reverse-recovery current. The battery, the coupled inductor (T_r) and the middle-voltage capacitor (C_2) connect in series to discharge into the HVSC through the high-voltage switch (S_3) by way of a low current type.

2.2.6 Mode 6 (t_5–t_6): At time $t = t_5$, the high-voltage switch (S_3) is turned off. After that, the body diode of the high-voltage switch (S_3) is turned on to carry the secondary current (i_{Ls}) because the stored energy in the coupled inductor (T_r) needs to release. In this mode, the battery, the coupled inductor (T_r) and the middle-voltage capacitor (C_2) still connect in series to discharge into the HVSC through the body diode of the high-voltage switch (S_3) by way of a low current type.

2.2.7 Mode 7 (t_6–t_7): At time $t = t_6$, this mode begins when the low-voltage switch (S_1) is triggered. As it cannot derive any currents from the paths of the HVSC, the middle-voltage circuit and the clamped circuit, the low-voltage switch (S_1) is turned on under the condition of zero-current-switching (ZCS) and this soft-switching property is helpful for alleviating the switching loss. As the rising rate of the current (i_{Lkp}) is limited by the primary-side leakage inductor (L_{kp}), and the secondary current (i_{Ls}) needs time to decay to zero, these two currents depend on each other. In this mode, the current flow is still directed to the HVSC, but its magnitude decreases gradually.

2.2.8 Mode 8 (t_7–t_8): At time $t = t_7$, the low-voltage switch (S_1) was turned on for a span and the secondary current (i_{Ls}) decays to zero. After that, the secondary current (i_{Ls}) reverses, and a large current passed through the secondary inductor (L_S) and the middle-voltage capacitor (C_2) to the low-voltage switch (S_1) is required to remove the residuary energy inside the body diode of the high-voltage switch (S_3). When the voltage across the high-voltage switch (S_3) is increasing and its value equals $V_{bus} - V_{C1}$, the diode (D_3) will be turned on. After that, it begins the next switching cycle and repeats the operation in mode 1.

For easy to analyse, the duty cycle of the low-voltage switch (S_1) is defined as d_1, and the other duty cycle d_3 of the high-voltage switch (S_3) is approximately equal to $1 - d_1$ by neglecting the dead time. Moreover, the coupling coefficient (k_p) is approximated to be one because the voltage gain is less sensitive to the coupling coefficient and the clamped capacitor (C_1) is appropriately selected to completely absorb the leakage inductor energy [18, 19]. When the low-voltage switch (S_1) is turned on, the voltage across the primary inductor (L_P) of the coupled inductor (T_r) can be represented as (17). Similarly, the voltage across the primary inductor (L_P) of the coupled inductor (T_r) can be represented as (20) when the low-voltage switch (S_1) is turned off. By using the voltage-second balance, the relation of the inductor voltage (v_{Lp}) can be represented via (17) and (20) as

$$(V_{bat} + V_{C2} - V_{C1})d_1 + (V_{bat} + V_{C2} - V_{bus})(1 - d_1) = 0 \quad (23)$$

The voltage gain (G_{V2}) of the proposed converter in the boost state can be obtained by (18), (22) and (23) as

$$G_{V2} = \frac{V_{bus}}{V_{bat}} = \frac{2 + N}{1 - d_1} \quad (24)$$

3 Design considerations

To verify the effectiveness of the designed topology, a 48 V battery module is utilised for the low-voltage source, and the desired output voltage is set at 360 V in the boost state. Moreover, a power supply is used to emulate a high-voltage dc bus ($V_{bus} = 360$ V), and the desired output voltage is set at 48 V in the buck state. Substituting $N = 1$–6 into (14), the curve of the voltage gain (G_{V1}) with respect to the duty cycle (d_3) is depicted in Fig. 4*a*. As can be seen from this figure, the voltage gain of the proposed bidirectional converter in the buck state is regulated via the conduction rate of the high-voltage switch (S_3), and the stable region of the duty cycle (d_3) is from zero to its maximum point. Hence, according to the manipulation of $\partial G_{V1}/\partial d_3 = 0$, the maximum controllable duty cycle equals

$$d_{3(max)} = \left(1 + \frac{1}{N}\right) - \sqrt{\frac{1}{N}\left(1 + \frac{1}{N}\right)} \quad (25)$$

Moreover, substituting $N = 1$–6 into (24), the curve of the voltage gain (G_{V2}) with respect to the duty cycle (d_1) is depicted in Fig. 4*b*. By analysing Figs. 4*a* and *b*, the turns ratio of the coupled inductor is selected as $N = 1.5$ when the operational conditions are $V_{bus} = 360$ V and $V_{bat} = 48$ V. Consequently, the corresponding duty cycles can be obtained as $d_3 = 0.45$ and $d_1 = 0.53$ by substituting $N = 1.5$ into (14) and (24). These values are reasonable in practical applications.

At the mode 1 of the buck state, the voltage across the low-voltage switch (S_1) can be obtained as $v_{S1} = V_{bat} - v_{Lp}$, in which the voltage across the primary inductor (v_{Lp}) according to the voltage-second balance can be given by $v_{Lp} = V_{bat}(d_1/d_3)$. Thus, the voltage across the low-voltage switch (S_1) can be rewritten as

$$v_{S1} = V_{bat}/d_3 \quad (26)$$

According to (14) and (26), the relations of the duty cycle (d_3), battery voltage (V_{bat}) and switch voltage (v_{S1})

© The Institution of Engineering and Technology 2011

doi: 10.1049/iet-pel.2011.0194

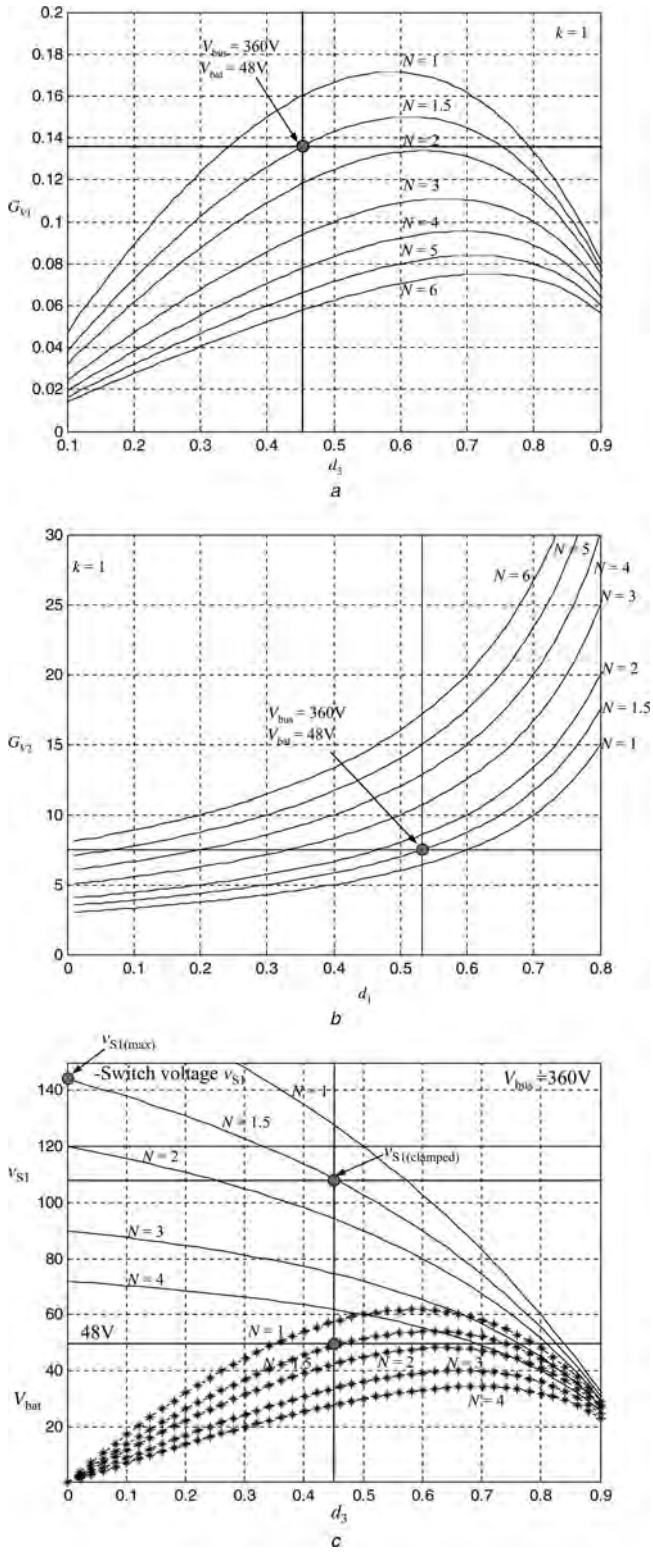

Fig. 4 *Voltage gain with respect to duty cycle under different turns ratios*

a Voltage gain (G_{V1}) with respect to duty cycle (d_3) under different turns ratios

b Voltage gain (G_{V2}) with respect to duty cycle (d_1) under different turns ratios

c Relationship of switch voltage (v_{S1}) and battery voltage (V_{bat}) with respect to duty cycle (d_3) under different turns ratios

under different turns ratios are illustrated in Fig. 4*c*. As can be seen from Fig. 4*c*, the maximum voltage stress across the switch (S_1) can be obtained when the duty cycle (d_3) is set at zero. In addition, according to (24) and (26), one can obtain

$$v_{S1} = V_{bus}/(N+2) \tag{27}$$

By analysing (27), the switch voltage (v_{S1}) is not related to the battery (V_{bat}) and the duty cycle (d_1) if the values of the voltage (V_{bus}) and the turns ratio (N) are fixed. Thus, the maximum sustainable voltage of the switch (S_1) is ensured to be constricted by the clamped capacitor ($V_{C1} = 102.8$ V). Moreover, the voltage across the middle capacitor is $V_{C2} = 174.8$ V by substituting $V_{C1} = 102.8$ V into (10). As long as the battery voltage is not higher than the voltage rating of the switch (S_1), the discharge mode can be applied well to different battery combinations. According to Fig. 4*c* and (27), the low-voltage switch (S_1) with 150 V rated-voltage is adopted in the buck and boost states.

At the mode 1 of the buck state, the series windings (L_P and L_S) can be taken as a single inductor, and the equivalent magnetising inductor (L_e) can be represented as $L_e = (1+N^2)L_P = (1+1/N^2)L_S$. If the ascendant slope of the magnetising current (di_{Le}/dt) is limited below 1.8 A/μs, the value of the equivalent magnetising inductor (L_e) can be determined as $L_e = 76.2$ μH according to the function of $L_e di_{Le}/dt = V_{bus} - V_{C2} - V_{bat}$. By considering the relationship of $L_e = (1+N^2)L_P = (1+1/N^2)L_S$ and the unconstrained coupling coefficient of $k = 0.95$, one can select the values of $L_P = 22$ μH and $L_S = 54$ μH in this study. Since the auxiliary inductor (L_2) is only operated in the buck state for releasing the energy stored in the leakage inductor, its design criterion is to ensure to be operated in the continuous current mode for preventing the step-down switch (S_2) and the diode (D_2) from a high current and limiting the current ripple. According to this consideration, the auxiliary inductor is chosen as $L_2 = 77$ μH by simulated examinations.

In this study, the clamped diode (D_1) should be a fast conductive device and its voltage rating is the same as the switch (S_1). Thus, the Schottky diode with lower consumptive power and conductive voltage may be a better choice. During the mode 3 in the buck state, the step-down switch current (i_{S2}) came from the currents (i_{C1} and i_{C2}) equals the inductor current (i_{L2}), the diode (D_2) is turned off and its voltage is given by $v_{D2} = V_{bat}/(1-d_3)$. According to the $d_{3(max)}$ in (25) and the operational conditions, the diode voltage (v_{D2}) is limited by three times of V_{bat}. Thus, a low-voltage Schottky diode can be adopted to conduct promptly with lower conduction loss and reverse-recovery current.

Owing to high switching frequency ($f_S = 100$ kHz) in the proposed bidirectional converter, the factors of lower equivalent series resistance and faster dynamic response should be considered in the design of the clamped capacitor (C_1) and the middle-voltage capacitor (C_2) for reducing capacitor voltage ripples. In this study, metalised-polyester film capacitors are adopted for C_1 and C_2. In order to further minimise the current and voltage ripples imposed to power switches (S_1, S_2 and S_3), the cutoff frequencies of the $L_P - C_1$ and $L_S - C_2$ filters are taken to be at least ten times smaller than the switching frequency [7]. According to the above consideration, the values of C_1 and C_2 are, respectively, chosen as 22 and 10 μF in this study so that the corresponding resonant frequencies are

$$f_{01} \equiv 1/(2\pi\sqrt{L_P C_1}) \cong 7.24\,\text{kHz}$$

$$f_{02} \equiv 1/(2\pi\sqrt{L_S C_2}) \cong 6.85\,\text{kHz}$$

© The Institution of Engineering and Technology 2011

In this study, the dc voltage feedback control is used to solve the problem of the output voltage varied with load variations, and a digital-signal-processor TMS320F2812 manufactured by Texas Instruments is adopted to achieve this goal of feedback control. In this feedback scheme, conventional proportional-integral (PI) control is utilised, and the corresponding PI gains are chosen to obtain the best dynamic characteristics in experimentations by considering the possible operating conditions. In the buck state, one control signal (V_{com3}) is produced by the PI controller according to the control objective of the voltage regulation for manipulating the driving signals (T_3). Moreover, the driving signal T_3 is generated by comparing the control signal V_{com3} with one carrier wave (v_{tri3}). The driving signals (T_1 and T_2) are complementary to the driving signal (T_3). On the other hand, one control signal (V_{com1}) is produced by the PI controller according to the control objective of the voltage regulation for manipulating the driving signals (T_1) in the boost state. In addition, the driving signal T_1 is generated by comparing the control signal V_{com1} with the other carrier wave (v_{tri1}), and the driving signal T_3 is complementary to the driving signal T_1 for the synchronous rectification. In order to avoid the overlap of the driving signals (T_1, T_2 and T_3), a dead time 0.15 μs is used in the experiments.

4 Experimental results

A prototype with the following specifications is designed in this section to illustrate the design procedure given in Section 3.

Low-side voltage: $V_{bat} = 48$ V;
High-side voltage: $V_{bus} = 360$ V;

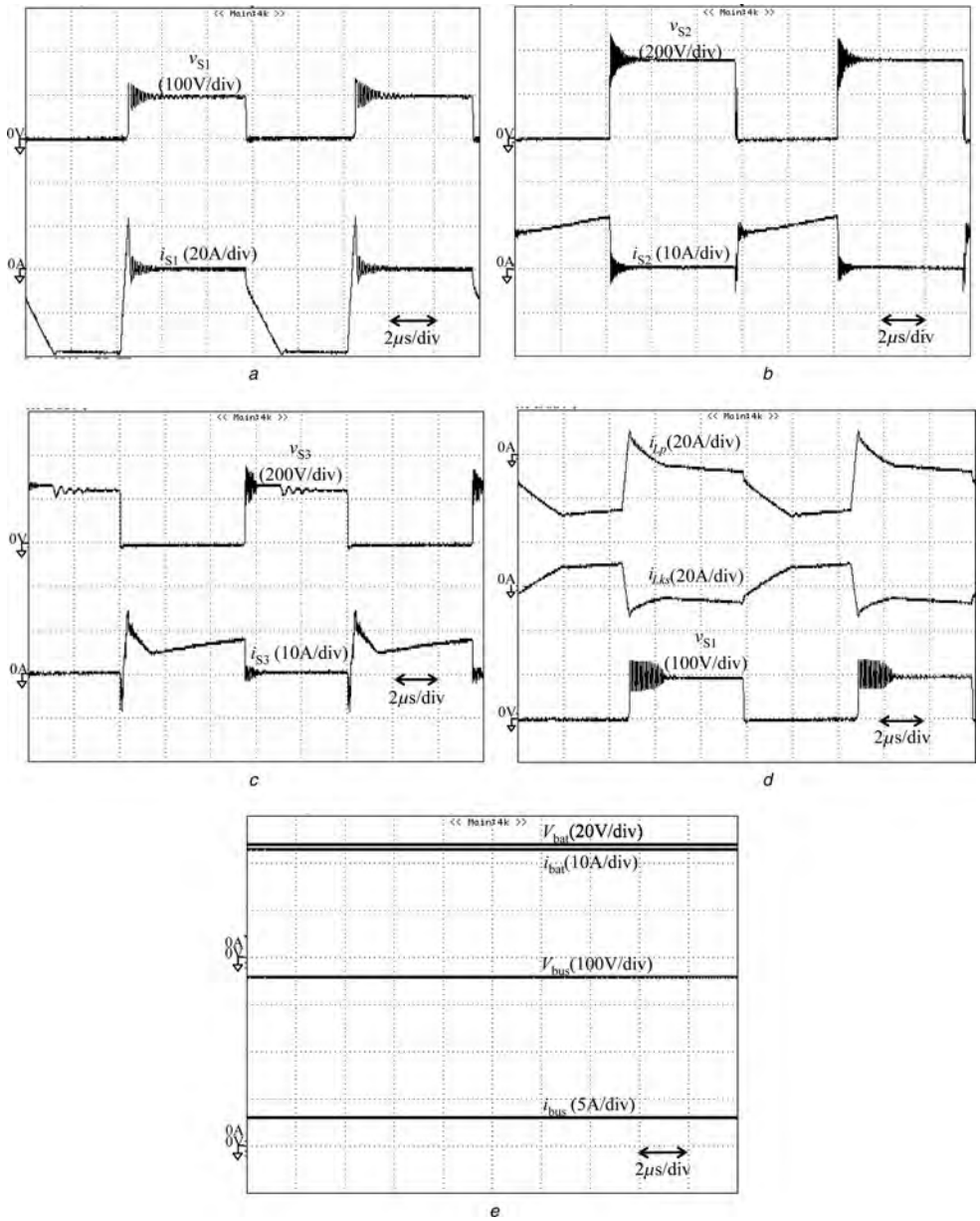

Fig. 5 *Experimental voltage and current responses of bidirectional converter in buck state with 1100 W-charge power*

a v_{S1} and i_{S1}
b v_{S2} and i_{S2}
c v_{S3} and i_{S3}
d i_{Lp}, i_{Lks} and v_{S1}
e V_{bat}, i_{bat}, V_{bus} and i_{bus}

© The Institution of Engineering and Technology 2011

doi: 10.1049/iet-pel.2011.0194

Switching frequency: $f_S = 100$ kHz;
Coupled inductor: $L_P = 22$ μH; $L_S = 54$ μH; N_1:$N_2 = 8$:12; $k = 0.95$; EE-55 core;
Switch: S_1: IRFPS3815 (150 V/105 A × 2, $R_{DS(on)} = 15$ mΩ); Super-247;
S_2, S_3: IXTQ 23N60Q (600 V/23 A × 2, $R_{DS(on)} = 0.32$ Ω); TO-3P;
Diode: D_1, D_2: Schottky diode SR20200CT, TO-220AB (200 V/20 A × 2);
D_3: Ultrafast rectifiers MUR1560CT, TO-220AC (600 V/15 A × 2);
Inductor: $L_2 = 77$ μH;
Capacitor: $C_1 = 22$ μF/100 V; $C_2 = 10$ μF/250 V;
$C_{bat} = 10$ μF/100 V × 7; $C_{bus} = 1$ μF/450 V × 10;
Weight: 2 kg;
Volume: 3750 cm^3 (25 cm × 15 cm × 10 cm).

The experimental voltage and current responses of the proposed bidirectional converter in the buck state operating at 1100 W-charge power are depicted in Fig. 5. From Fig. 5*a*, the switch voltage (v_{S1}) is clamped at 100 V, which is much smaller than the high-side voltage ($V_{bus} = 360$ V). By observing Figs. 5*b* and *c*, the voltages across the switches (S_2 and S_3) are clamped under 360 V, and the switches (S_2 and S_3) are turned on with ZVS. As can be seen from Fig. 5*d*, the primary current (i_{Lp}) is higher than the current (i_{Lks}) so that the full copper film is utilised in the primary side, but usual enamel-insulated wires could be used in the secondary winding. By observing Fig. 5*e*, the low-side voltage can be stably adjusted by a proportional-integral (PI) voltage controller to be $V_{bat} = 48$ V as the high-side voltage is $V_{bus} = 360$ V. The effects of the proposed converter operating in the buck state due to the varied high-side voltage and the output power variation are given in Fig. 6, where the response of $V_{bus} = 350$ V with 1100 W-charge power is depicted in Fig. 6*a*; the response of $V_{bus} = 370$ V with 1100 W-charge power is depicted in Fig. 6*b*; the response of the output power variation between 500 and 900 W is depicted in Fig. 6*c*. By observing Fig. 6, the low-side voltage $V_{bat} = 48$ V is insensitive to the varied high-side voltage and the output power variation owing to the PI closed-loop voltage control.

Fig. 7 shows the voltage and current responses of the proposed bidirectional converter in the boost state operating at 1200 W-discharge power. From Fig. 7*a*, the switch voltage (v_{S1}) is clamped at 100 V that is much smaller than the high-side voltage ($V_{bus} = 360$ V). According to Figs. 7*b* and *c*, the salient features of high-voltage elements with lower current and low-voltage elements with higher current can be verified. By observing Fig. 7*d*, the high-side voltage can be stably adjusted by a conventional PI voltage controller to be $V_{bus} = 360$ V when the low-side voltage is $V_{bat} = 48$ V. The effects of the proposed converter operating in the boost state due to the varied low-side voltage and the output power variation are given in Figs. 7*e*–*g*, where the response of $V_{bat} = 40$ V with 1200 W-discharge power is depicted in Fig. 7*e*; the response of $V_{bat} = 56$ V with 1200 W-discharge power is depicted in Fig. 7*f*; the response of the output power variation between 800 and 1200 W is depicted in Fig. 7*g*. By observing Figs. 7*e*–*g*, the high-side voltage $V_{bus} = 360$ V is insensitive to the varied low-side voltage and the output power variation owing to the PI closed-loop voltage control.

Fig. 8 summarises the experimental conversion efficiency of the proposed converter in the buck and boost states,

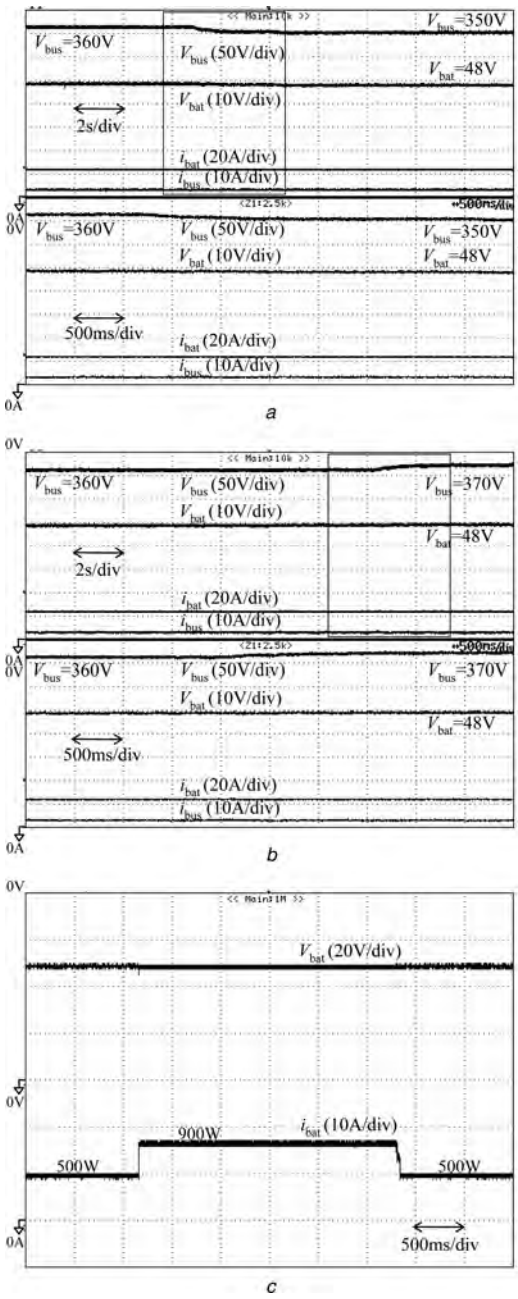

Fig. 6 *Experimental input/output voltage and current responses of bidirectional converter in buck state due to varied voltage and output power*

a $V_{bus} = 350$ V with 1100 W-charge power
b $V_{bus} = 370$ V with 1100 W-charge power
c Output power variation between 500 and 900 W

where the conversion efficiency in the buck state is depicted in Fig. 8*a*, and the one in the boost state is depicted in Fig. 8*b*. In the experiments, the converter efficiency is evaluated via Power Analyzer PA4400A equipment, manufactured by the AVPower Company. The bandwidth of the PA4400A is dc to 500 kHz, and the accuracy of the measured power is within ±0.1%. From the experimental results, the efficiency in the boost state is higher than the one in the buck state under light power because the former only uses two power switches. The maximum conversion efficiency of the proposed bidirectional converter both in the buck and boost states are over 95%; the measured charge and discharge powers are about 1.15 and 2 kW, respectively.

© The Institution of Engineering and Technology 2011

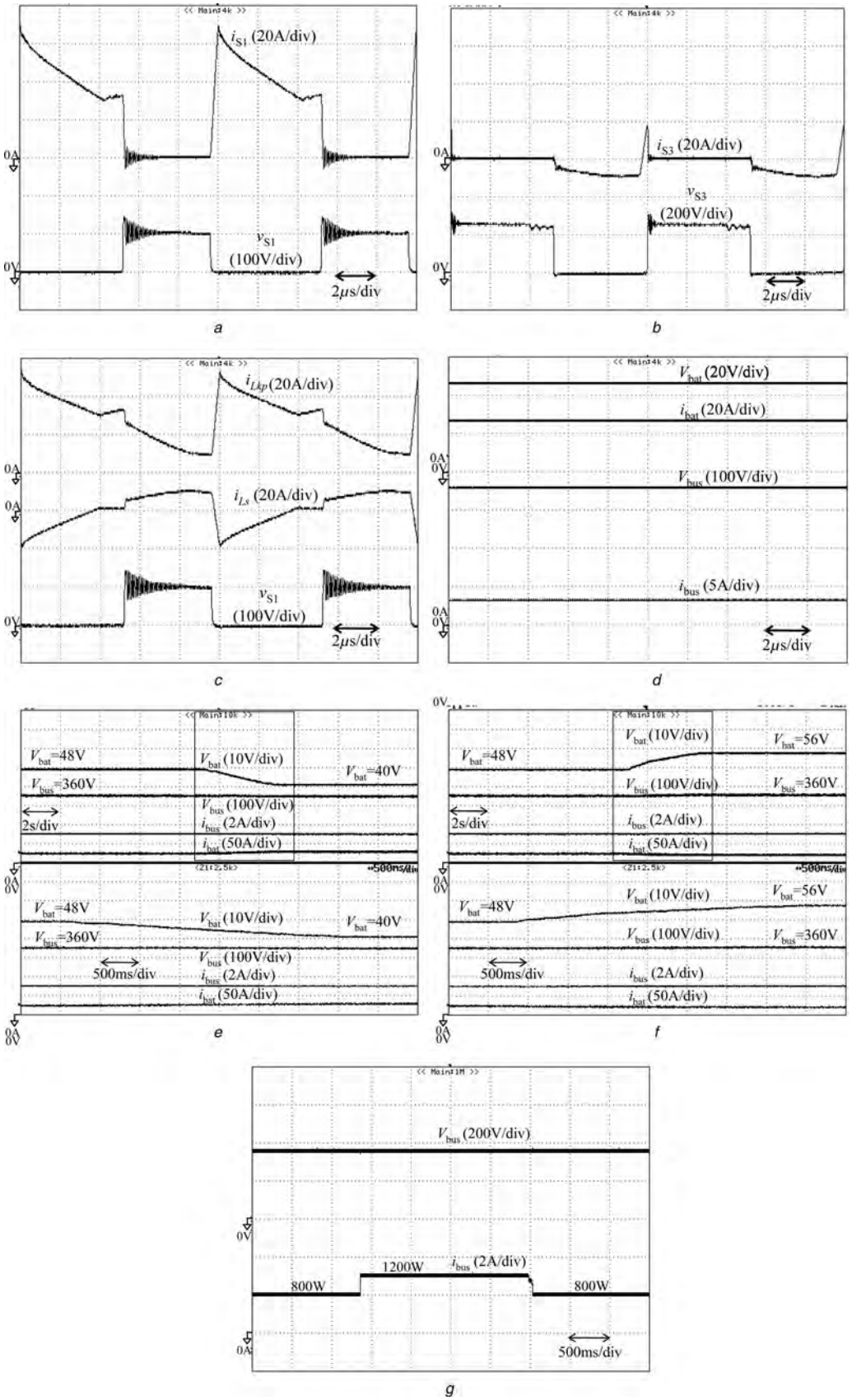

Fig. 7 *Experimental voltage and current responses of bidirectional converter in boost state with 1200 W-discharge power*

a v_{S1} and i_{S1}
b v_{S3} and i_{S3}
c i_{Lkp}, i_{Ls} and v_{S1}
d V_{bat}, i_{bat}, V_{bus} and i_{bus}
e Response due to $V_{bat} = 40$ V
f Response due to $V_{bat} = 56$ V
g Output power variation between 800 W and 1200 W

© The Institution of Engineering and Technology 2011

doi: 10.1049/iet-pel.2011.0194

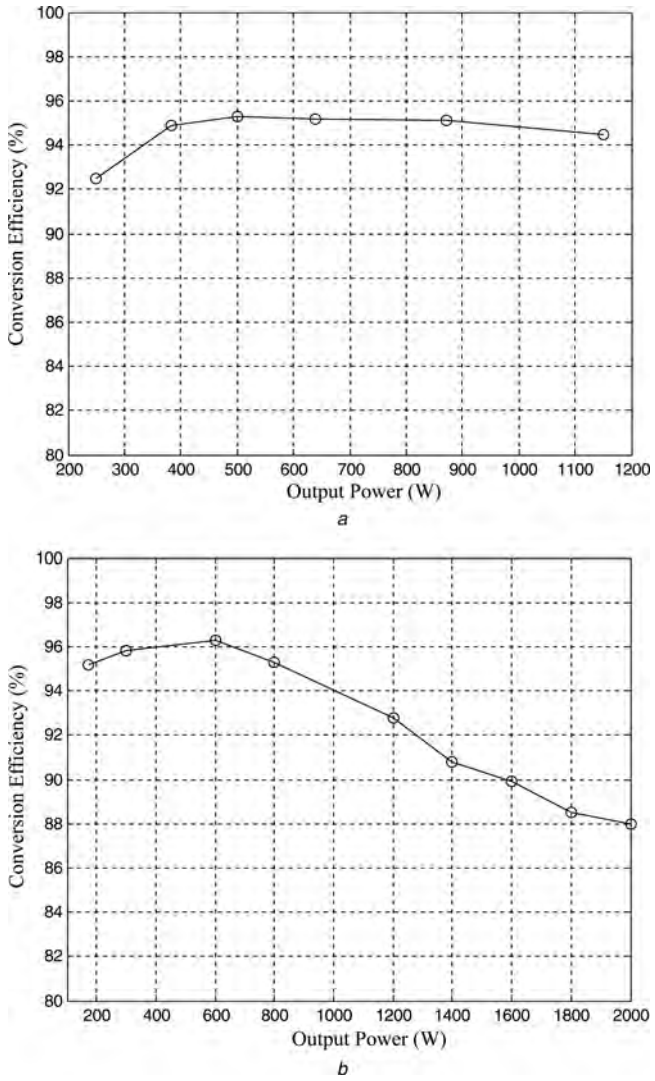

Fig. 8 *Conversion efficiency of bidirectional converter for* $V_{bat} = 48$ *V and* $V_{bus} = 360$ *V under different powers*

a Buck state
b Boost state

According to the maximum output power 2 kW with the corresponding conversion efficiency 88%, the magnetising current of the coupled inductor should be designed to sustain the maximum value of 45.98 A/0.88 ≒ 52.26 A by substituting $d_1 = 0.53$ and $N = 1.5$ into $i_{Lmp} = i_{bat}[(1 + N)/(2 + Nd_1 - d_1)]$. In this study, the EE-55 core with an air gap of 2 mm, eight primary winding turns, the magnetic flux density 390 mT and the cross-section area 354 mm^2 are used to fabricate the coupled inductor. According to the specification of the EE-55 core, this design can sustain the maximum magnetising current of 75 A. Thus, it can prevent the saturation phenomenon of the magnetising current. In the proposed bidirectional dc–dc converter, the energy is translated by the magnetising inductor of the coupled inductor, not a transformer. The magnetic energy of the coupled inductor always has a path to release, and the operation principle is similar to a flyback converter. Therefore the imbalance phenomenon of the magnetising current will not exist in the proposed topology.

The performance comparisons of the proposed bidirectional dc–dc converters with similar researches in the announced works are summarised in Table 1. As can be seen from the tabulable data, the maximum conversion efficiency of the previous bidirectional dc–dc converters in [12] and [22] is slightly higher than the proposed one in this study. However, the amounts of power switches in [12] and [22] are over double than the requirement in the proposed converter. It will result in the increase of manufacturing cost. Thus, the proposed bidirectional dc–dc converter indeed performs high conversion efficiency and bidirectional power flow under a 2 kW level output power with less power switches than other announced works [5, 6, 9, 12, 14, 22].

5 Conclusions

This study developed a high-efficiency bidirectional dc–dc converter, and this coupled-inductor converter was applied well to a low-voltage-type battery. The experimental results reveal that the maximum efficiency was measured to exceed 95%, and the average conversion efficiency was measured over 92.5% both in the buck and boost states. The newly designed converter circuit offers the following improvement over those reported elsewhere: (i) This topology adopts only three switches to achieve the objective of bidirectional power flow. (ii) The voltage gain and the utility rate of the magnetic core can be substantially increased by using a coupled inductor with a lower turns ratio. (iii) The stray

Table 1 Performance comparisons with other announced works

References	Input voltage	Output voltage	Output power	Maximum conversion efficiency	Amount of power switches
[5]	5 V	9 V	20 W	Step-up 85% Step-down 80%	4
[6]	50 V	360 V	200 W	Step-up 87% Step-down 91%	4
[9]	24 V	24 V	60 W	Step-up 93% Step-down 94%	4
[12]	12 V	300 V	2 kW	Step-up 96% Step-down 96%	9
[14]	14 V	42 V	60 W	Step-up 95% Step-down 94%	7
[22]	48 V	400 V	500 W	Step-up 96.5% Step-down 96%	8
This work	48 V	360 V	2 kW	Step-up 96.3% Step-down 95.3%	3

© The Institution of Engineering and Technology 2011

energy can be recycled by a clamped capacitor into the battery or high-voltage side to ensure the property of voltage clamping. (iv) When this circuit operates only in the boost state, the switch voltage stress is not related to the input voltage, and it is therefore more suitable for a dc power conversion mechanism with different battery combinations. (v) The copper loss in the magnetic core can be greatly reduced as a full copper film with lower turns. This high-efficiency converter topology provides designers with an alternative choice for converting various power sources efficiently. It can also be extended easily to other power conversion systems to meet the demand for a wide range of voltages.

6 Acknowledgments

This work was supported in part by the National Science Council of Taiwan, ROC through grant number NSC 100-3113-E-155-001. Moreover, the authors would like to express their gratitude to the referees and the associate editor for their useful comments and suggestions.

7 References

1 Pascual, C., Krein, P.T.: 'Switched capacitor system for automatic series battery equalization'. IEEE Applied Power Electronics Conf., 1997, vol. 2, pp. 848–852
2 Giess, H.: 'The operation of VRLA lead acid batteries in parallel strings of dissimilar capacity or Can we now sin?'. IEEE Telecommunications Energy Conf., 1999, pp. 18.1.1–18.1.5
3 Xu, D.H., Zhao, C.H., Fan, H.F.: 'A PWM plus phase-shift control bidirectional DC-DC converter', *IEEE Trans. Power Electron.*, 2004, **19**, pp. 666–675
4 Peng, F.Z., Li, H., Su, G.J., Lawler, J.S.: 'A new ZVS bidirectional DC-DC converter for fuel cell and battery application', *IEEE Trans. Power Electron.*, 2004, **19**, pp. 54–65
5 Chung, H.S.H., Chow, W.C., Hui, S.Y.R., Lee, S.T.S.: 'Development of a switched-capacitor DC-DC converter with bidirectional power flow', *IEEE Trans. Circuits Syst.*, 2000, **47**, pp. 1383–1389
6 Jain, M., Daniele, M., Jain, P.K.: 'A bidirectional DC-DC converter topology for low power application', *IEEE Trans. Power Electron.*, 2000, **15**, pp. 595–606
7 Schuch, L., Rech, C., Hey, H.L., Gründling, H.A., Pinheiro, H., Pinheiro, J.R.: 'Analysis and design of a new high-efficiency bidirectional integrated ZVT PWM converter for DC-bus and battery-bank interface', *IEEE Trans. Ind. Appl.*, 2006, **42**, (5), pp. 1321–1332
8 Chan, H.L., Cheng, K.W.E., Sutanto, D.: 'ZCS-ZVS bi-directional phase-shifted DC-DC converter with extended load range', *IEE Proc. Electr. Power Appl.*, 2003, **150**, pp. 269–277
9 Chen, G., Lee, Y.S., Hui, S.Y.R., Xu, D.H., Wang, Y.S.: 'Actively clamped bidirectional flyback converter', *IEEE Trans. Ind. Electron.*, 2000, **47**, pp. 770–779
10 Zhu, L.: 'A novel soft-commutating isolated boost full-bridge ZVS-PWM DC-DC converter for bidirectional high power applications', *IEEE Trans. Power Electron.*, 2006, **21**, (2), pp. 422–429
11 Lee, J., Jo, J., Choi, S., Han, S.B.: 'A 10-kw SOFC low-voltage battery hybrid power conditioning system for residential use', *IEEE Trans. Energy Convers.*, 2006, **21**, (2), pp. 575–585
12 Chiu, H.J., Lin, L.W.: 'A bidirectional DC-DC converter for fuel cell electric vehicle driving system', *IEEE Trans. Power Electron.*, 2006, **21**, (4), pp. 950–958
13 Ma, G., Qu, W., Yu, G., Liu, Y., Liang, N., Li, W.: 'A zero-voltage-switching bidirectional DC-DC converter with state analysis and soft-switching-oriented design consideration', *IEEE Trans. Ind. Electron.*, 2009, **56**, (6), pp. 2174–2184
14 Lee, Y.S., Chiu, Y.Y.: 'Zero-current-switching switched-capacitor bidirectional DC-DC converter', *IEE Proc. Electr. Power Appl.*, 2005, **152**, (6), pp. 1525–1530
15 Lee, Y.S., Chiu, Y.Y.: 'Switched-capacitor quasi-resonant step-up/step-down bidirectional converter', *Electron. Lett.*, 2005, **41**, (15), pp. 1403–1404
16 Zhao, Q., Lee, F.C.: 'High-efficiency, high step-up DC-DC converters', *IEEE Trans. Power Electron.*, 2003, **18**, pp. 65–73
17 Inaba, C.Y., Konishi, Y., Nakaoka, M.: 'High frequency PWM controlled step-up chopper type DC-DC power converters with reduced peak switch voltage stress', *IEE Proc. Electr. Power Appl.*, 2004, **151**, pp. 47–52
18 Wai, R.J., Duan, R.Y.: 'High-efficiency DC/DC converter with high voltage gain', *IEE Proc. Electr. Power Appl.*, 2005, **152**, pp. 793–802
19 Wai, R.J., Duan, R.Y.: 'High step-up converter with coupled-inductor', *IEEE Trans. Power Electron.*, 2005, **20**, pp. 1025–1035
20 Yu, W., Qian, H., Lai, J.S.: 'Design of high-efficiency bidirectional DC-DC converter and high-precision efficiency measurement', *IEEE Trans. Power Electron.*, 2010, **25**, (3), pp. 650–658
21 Wu, T.F., Chen, Y.C., Yang, J.G., Kuo, C.L.: 'Isolated bidirectional full-bridge dc-dc converter with a flyback snubber', *IEEE Trans. Power Electron.*, 2010, **25**, (7), pp. 1915–1922
22 Chen, W., Rong, P., Lu, Z.: 'Snubberless bidirectional DC-DC converter with new CLLC resonant tank featuring minimized switching loss', *IEEE Trans. Ind. Electron.*, 2010, **57**, (9), pp. 3075–3086

© The Institution of Engineering and Technology 2011

doi: 10.1049/iet-pel.2011.0194